

# Color Differences Highlight Concomitant

## Polymorphism of Chalcones

*Charlie L. Hall<sup>1</sup>, Rui Guo<sup>2</sup>, Jason Potticary<sup>1</sup>, Matthew E. Cremeens<sup>3</sup>, Stephen D. Warren<sup>3</sup>,  
Iryna Andrusenko<sup>4</sup>, Mauro Gemmi<sup>4</sup>, Martijn A. Zwijnenburg<sup>2</sup>, Hazel A. Sparkes<sup>1</sup>, Natalie E.  
Pridmore<sup>1</sup>, Sarah L. Price<sup>2</sup>, Simon R. Hall<sup>1\*</sup>*

<sup>1</sup> University of Bristol, School of Chemistry, Cantock's Close, Bristol BS8 1TS, U.K.

<sup>2</sup> Department of Chemistry, University College London, 20 Gordon Street, London WC1H 0AJ, U.K.

<sup>3</sup> Department of Chemistry and Biochemistry, Gonzaga University, 502 E. Boone Avenue, Spokane, WA 99258, United States.

<sup>4</sup> Center for Nanotechnology Innovation@NEST, Istituto Italiano di Tecnologia, Piazza San Silvestro 12, Pisa, Italy.

**ABSTRACT** The *meta*- and *para*- nitro isomers of (*E*)-3'-dimethylamino-nitrochalcone (Gm8m and Gm8p) are shown to exhibit concomitant color polymorphism, with Gm8m appearing as yellow ( $P2_1/c$ ) or orange ( $P-1$ ) crystals and Gm8p appearing as red ( $P2_1/n$ ) or black ( $P2_1/c$ ) crystals. Each of the polymorphs were characterized optically via UV-Vis spectroscopy and their thermal behavior via differential scanning calorimetry and low temperature powder X-ray diffraction. To assess the effect of molecular configuration and crystal packing on the colors of crystals of the different polymorphs, time dependent DFT ( $\omega$ B97x) calculations were carried out on isolated molecules, dimers, stacks and small clusters cut from the crystal structures of the four polymorphs. The calculated color comes from several excitations and is affected by conformation and most intermolecular contacts within the crystal, with the color differences between polymorphs mainly being due to the

differences in the  $\pi - \pi$  stacking. The visual differences between these related polymorphic systems make them particularly useful for studying polymorph behavior such as phase transitions and concomitant polymorph growth.

## INTRODUCTION

Polymorphism is now an extensively studied phenomenon for its relevance in the manufacturing of specialty chemicals, such as pharmaceuticals, due to the many physical properties that may differ between crystal structures.<sup>1, 2</sup> Any variation in color between polymorphs makes it particularly easy to spot polymorphic systems, which is why the ten polymorphs of ROY (5-methyl-2-[(2-nitrophenyl)amino]-3-thiophenecarbonitrile) are so often used to illustrate the phenomena of polymorphism and the challenges in characterizing large numbers of crystal structures.<sup>3-6</sup>

Chalcones ((2*E*)-1,3-diphenylprop-2-en-1-ones) are naturally occurring compounds that are present in several organisms and show significant activity within them, so are a widely used scaffold in medicinal chemistry.<sup>7</sup> They are used as antioxidants,<sup>8</sup> anti-inflammatories,<sup>9</sup> and show antibacterial properties<sup>10</sup> to tackle infections such as stomach ulcers,<sup>11</sup> and have been investigated as anti-cancer treatments for necrosis of cells,<sup>12</sup> as well as prevention of cell division.<sup>13</sup> A chalcone derivative has been investigated for inhibition of age-related osteoporosis,<sup>14</sup> others as diabetes treatment drugs<sup>15</sup> and asthma prevention.<sup>16</sup> Agrochemical uses are the prevention of fungal/insect infestation,<sup>17</sup> as well as for viral prevention.<sup>18</sup> It is thought that the main active functional group of these compounds is the  $\alpha,\beta$  unsaturated ketone.<sup>19</sup> This functional region conjugates the two aromatic rings, the 1-ring and the 3-ring (**Figure 1**), of the molecule to allow electronic interactions that directly affect molecular conformation and color. Indeed, the name chalcone comes from the tendency of the molecules to be colored, from the Greek word *chalcos* for bronze.<sup>20</sup> Hence the chalcone core

is a relatively large conjugated system that is a model for the properties of pharmaceuticals that are linked to the  $\pi$  system, in the way that pentacene is seen as the model system for organic opto-electronics.<sup>21-24</sup>

As part of a systematic study of crystallographic packing, a wide range of substituted chalcones have been synthesized. In general, the addition of functional groups to chalcones results in crystals differing only marginally in color from the unsubstituted chalcone. However, the introduction of electron donating substituents, such as a dimethylamino- group, onto either ring of the chalcone results in clear optical changes. Here we report the structural solution of two polymorphic isomers (**Figure 1**) – 3'-dimethylamino-3-nitrochalcone (Gm8m) and 3'-dimethylamino-4-nitrochalcone (Gm8p) which, when recrystallized from acetone, both exhibit concomitant polymorphism of crystals differing in color and morphology.

This system of four polymorphs exhibits colors ranging across the optical spectrum (**Figure 2**) and thus raises the questions as to the cause of such color polymorphism (also called crystallochromy).<sup>25, 26</sup> The color of organic molecules, whether in solution or as crystals, arises from the light that does not get absorbed by the molecules, as only that light, be it through reflection or transmission, reaches the observer's eyes. The absorption of light by molecules is the result of the excitation of electrons from occupied to unoccupied orbitals. The longest wavelength, lowest energy, excitation is especially relevant as any light with a longer wavelength will not be absorbed and contributes to the observed color. For example, a molecule with a longest wavelength excitation in the orange will likely appear red with all or most of the shorter wavelength light absorbed and only the red light completely reflected or transmitted.

In the gas phase, the molecules are sufficiently separated that molecular absorption spectra can be predicted by calculations on an isolated molecule. In solution, the peaks of the

spectrum will shift (solvatochromism) and buffeting of the molecules by the solvent leads to homogenous and inhomogeneous broadening, losing the sharp vibronic transitions seen for the isolated molecule in the gas phase. When the color of a solution depends on the solvent, this may reflect differences to the degree that the ground state and excited states of the molecules are stabilized by the solvent, but may also include charge transfer to solvent molecules, or different degrees of aggregation of the solute molecules. When going from solution to the solid-state, the absorption spectrum of a molecule can shift both due to changes in the conformation of the molecule induced by packing, and because of electronic interactions between close-packed molecules.<sup>27</sup>

The variation in color of ROY and other polymorphic systems have been attributed to the differences in the conformation of the molecule and hence the  $\pi$  delocalisation.<sup>28-31</sup> Similarly, differences in the position of the nitrogen lone pair relative to the aromatic rings were used to rationalize the color variations in the polymorphs of picrytoluidine.<sup>32</sup> In contrast, in the case of rigid perylene derivatives,<sup>25,26</sup> which lack conformational degrees of freedom, the variation in color has been explained purely in terms of differences of crystal packing and  $\pi$  stacks, which are generally well defined in the crystals of such rigid molecules. The cause of color variations in polymorphs of cocrystals, when the crystals of the components are colorless, has been rationalized in terms of the different intermolecular interactions between the component molecules in the crystal structures.<sup>33,34</sup>

Hence, we report the preparation, crystal structures, relative stability and spectral properties of two pairs of polymorphs of chalcone isomers, and a limited polymorph screen. This experimental characterization is used to assess current methods of modelling organic polymorphs of two molecules whose charge distributions are very similar (**Figure 1**). In particular, we assess the extent to which current computational methods can account for the

differences in the colors of the polymorphs, and how this relates to the challenges of modelling the properties of crystals of conjugated molecules.

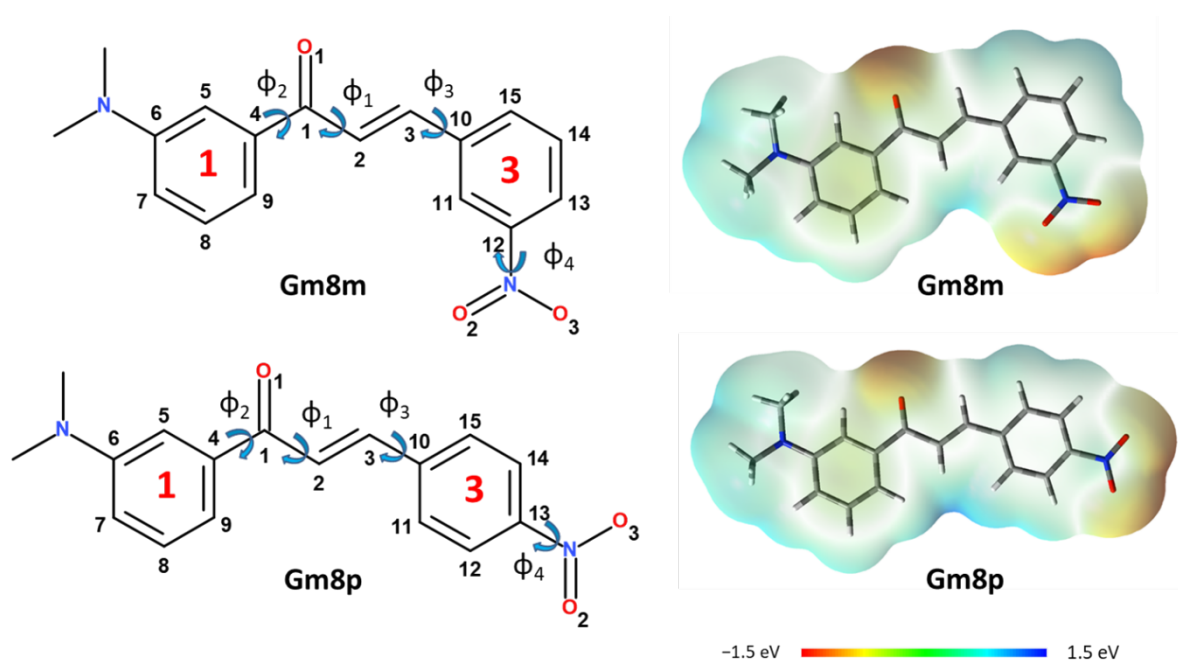


**Figure 1.** Molecular structure of Gm8m and Gm8p. The naming and labelling are from our ongoing work in generating a library of chalcone crystal structures. The flexibility of the molecules was characterized through torsion angles defined as  $\Phi_1$ : C4-C1-C2-C3,  $\Phi_2$ : C5-C4-C1-C2,  $\Phi_3$ : C15-C10-C3-C2,  $\Phi_4$ : O2-N-C12-C11 (left). Electrostatic potential maps (B3LYP/6-311++G(2d,p)) were plotted on the 0.0004 SCF density surface for the optimized isolated molecules.

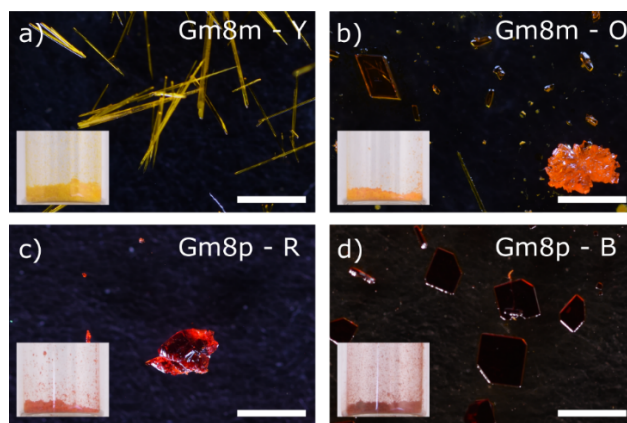


**Figure 2.** Optical images of crystals of a) Gm8m – Y, b) Gm8m – O, c) Gm8p – R, d) Gm8p – B. All scale bars represent 1 mm. Insets show a powdered sample of each crystal.

## METHODS

### *Synthesis of Functionalized Chalcones*

(*E*)-1-[3-(dimethylamino)phenyl]-3-(3-nitrophenyl)prop-2-en-1-one, or 3'-dimethylamino-3-nitrochalcone (Gm8m) and (E)-1-[3-(dimethylamino)phenyl]-3-(4-nitrophenyl)prop-2-en-1-one, or 3'-dimethylamino-4-nitrochalcone (Gm8p) were synthesized via a base-catalyzed aldol condensation reaction between a nitro-substituted benzaldehyde and dimethylamino-substituted acetophenone (Supporting Information 1.1). The compounds were recrystallized from ethanol and analyzed via NMR (Supporting Information Figure 1-2).

### *Preparation of Polymorphs*

Crystals of both polymorphs of Gm8m and Gm8p grew concomitantly via evaporation from 40 mg.mL<sup>-1</sup> solutions in acetone. Crystals large enough to analyze via single crystal X-ray diffraction (sc-XRD) were produced for Gm8m orange (Gm8m – O), Gm8p red (Gm8p – R) and Gm8p black (Gm8p – B). Crystals suitable for sc-XRD of the yellow polymorph of Gm8m (Gm8m – Y) were produced via slow evaporation of a 10 mg.mL<sup>-1</sup> solution in ethanol. For the isolation of individual polymorphs, a solvent screen was carried out to find the

optimal conditions for the individual growth of each polymorph (Supporting Information 1.2).

### ***Single Crystal X-ray Diffraction***

Sc-XRD data for all samples were acquired using a Bruker Apex II CCD diffractometer using Mo K $\alpha$  radiation ( $\lambda = 0.71073 \text{ \AA}$ ). Intensities were integrated in SAINT<sup>35</sup> and absorption corrections based on equivalent reflections were carried out using SADABS.<sup>36</sup> Structural solution was carried out in Olex2<sup>37</sup> using Superflip<sup>38, 39</sup> and refined in SHELXL.<sup>40</sup> Crystallographic data is shown in Supporting Information Table 9. Unless stated, diffraction data was collected at 100 K.

### ***Powder X-ray Diffraction***

Powder X-ray diffraction (p-XRD) data was collected using a Bruker D8 Advance diffractometer (Cu-K $\alpha$  1.5418  $\text{\AA}$ ) with a PDS LynxEye Detector attachment. Samples were ground using pestle and mortar before measurements and placed on a low-background silicon wafer holder. Scans were taken over the  $2\theta$  range 5-50° at a rate of 0.75° .min<sup>-1</sup> and compared to sc-XRD data simulated using Mercury.<sup>41</sup>

### ***UV-Vis Spectroscopy***

Solid-state and solution UV-Vis spectroscopy used a Perkin Elmer Lambda 650 spectroscope at room temperature. Solution based measurements were taken using 10 mm path length quartz cuvettes. Concentrations from 0.5-0.008 mg.mL<sup>-1</sup> were analyzed, which were prepared consecutively by dilution. Dry solvents (>99%) were used in all cases. Solid-state diffuse reflectance measurements were carried out using a 60 mm integrating sphere attachment to the spectrometer. Solid samples were crushed with a pestle and mortar before being added to

the sample holder. p-XRD was carried out on the crushed samples to confirm that no polymorphic transition had occurred during the preparation process.

### ***Differential Scanning Calorimetry***

Differential scanning calorimetry (DSC) was carried out using a TA Instruments Discovery DSC25. The cell was purged with N<sub>2</sub> gas at a rate of 50 mL.min<sup>-1</sup>. Samples (2-10 mg) were weighed out and sealed in Tzero aluminum pans. Samples were run through heat-cool-heat cycles starting at 30°C, to temperatures at least 10°C above the melting endotherms observed. In general, the cooling ramps were down to 0°C, however for the observation of glass transitions of Gm8m, runs to -70°C were carried out. TRIOS software (version: 4.5.0.42498) was used for analysis of thermograms. Endothermic and exothermic transition onsets are reported at extrapolated onset, and glass transitions at the midpoint of the transition. Enthalpy values were calculated using a linear baseline. Temperature and cell constant calibrations were carried out using a certified indium standard (verification: Temperature = 156.6±0.5°C, Enthalpy = 28.72 J.g<sup>-1</sup> ± 4%).

### ***Computational Modelling***

The electronic structure of pharmaceutical crystals is usually calculated using periodic density functional theory,<sup>42</sup> employing the PBE functional and a variety of dispersion corrections. Although the PBE functional is known to be poor at describing delocalized systems,<sup>43,44</sup> including the conformations within some ROY polymorphs,<sup>3</sup> GGA functionals like PBE are usually the most accessible method that can be used either for many hundreds of structures in a crystal structure prediction study, or to estimate the free energy by harmonic phonon calculations. Thus all four crystal structures were optimized in CASTEP<sup>45</sup> using PBE<sup>46</sup> with the TS dispersion correction.<sup>47</sup> The lattice energies at these geometries were also calculated with a many-body dispersion correction MBD\*,<sup>48</sup> as well as Grimme's D02<sup>49</sup> and D03<sup>50</sup> dispersion corrections. The harmonic phonons were calculated to estimate the free

energy (Supporting Information 2.3). The diamagnetic susceptibility tensor was also calculated with CASTEP using PBE.<sup>51</sup> However, this functional is known to be very poor for band gaps of insulators and semi-conductors<sup>52</sup> and by extension their optical properties (as confirmed in Supporting Information 2.4). Therefore, a range-separated functional was used when calculating the optical properties (see below).

As the ability to calculate optical properties is more developed in molecular than periodic quantum chemistry codes, and because we were interested to explore the difference between the optical properties of isolated molecules and the crystalline polymorphs, we used non-periodic calculations to predict absorption spectra. Time dependent density functional theory (TD-DFT) calculations were performed using Gaussian09<sup>53</sup> and Turbomole 7.4,<sup>54</sup> the  $\omega$ B97X density functional,<sup>55</sup> the 6-31G(d,p) basis set<sup>56</sup> and from six to thirty excited states, on isolated molecules and molecular clusters cut from the crystalline polymorphs. TD-DFT goes beyond the orbital energy difference approximation, where spectral features are assumed to arise from excitation of single electrons from occupied to unoccupied orbitals, such as the HOMO to LUMO, with everything else staying the same, and properly includes the full electronic relaxation resulting from exciting an electron. Use of range-separated functionals, such as  $\omega$ B97X, is essential as they allow for a balanced treatment of local and charge-transfer excited states, even if slightly blue-shifting the whole spectrum.<sup>57</sup> In spectra calculated with a GGA functional, like PBE, the charge-transfer excited states would be spuriously stabilized resulting in the wrong ordering of excited states and a significant overestimation of the effect of stacking.<sup>58</sup> The Turbomole TD-DFT calculations additionally made the resolution of the identity (RI) approximation, which was shown to have a negligible effect on the calculated spectra (Supporting Information 2.5.4.8). Calculations on isolated molecules with the larger 6-311++G(2d,p) basis-set, suggest that increasing the basis-set has only a small effect on the calculated spectra (Supporting Information 2.5.2). Molecular

clusters were extracted from the crystal structures optimized with CASTEP using Mercury. UV-Vis spectra were produced from TD-DFT excitations by combining Gaussian functions with a full width at half-maximum of 0.3 eV, centered at each excitation energy, with peak area proportional to corresponding oscillator strength from TD-DFT calculations. In order to understand the nature of the transitions, molecular orbitals involved in the TD-DFT transitions were visualized using GaussView<sup>59</sup> (Supporting Information Table 21).

## EXPERIMENTAL CHARACTERISATION

### *Polymorphs of Gm8m and Gm8p*

The structures of Gm8m and Gm8p polymorphs were solved via sc-XRD, confirming the existence of at least two polymorphs of each molecule. Yellow needle-like crystals (Gm8m – Y) and orange block-like crystals (Gm8m – O) were isolated for Gm8m. Black block-like crystals (Gm8p – B), which appear dark red when ground into a powder, and red needle-like crystals (Gm8p – R) were used for structure solution, though red plate and block crystals were often in the samples (Supporting Information 1.2). A third orange polymorph of Gm8p was also isolated (Gm8p – O), however sc-XRD was not possible due to poor crystallinity of the sample. The structure of Gm8p – O was partially analyzed using a combination of 3D electron diffraction<sup>60</sup> and crystal structure prediction, however an exact structural solution was not acquired (Supporting Information 1.6). Gm8m – Y showed a level of disorder within the structure (0.862:0.138 occupancies at 100 K) which increased with temperature, via a small twisting of the nitro-group (Supporting Information 1.4).

For optical and thermal characterization, it was necessary to produce phase pure samples of each polymorph. For the isolation of individual polymorphs in quantifiable amounts, a polymorph screen was carried out using a variety of solvents, concentrations and magnetic fields. Calculations showed differences in the magnetic anisotropy of each polymorph of

Gm8m and Gm8p (Supporting Information 2.6), which has been suggested to be the cause of polymorph selectivity for a selection of organic systems.<sup>51</sup> However, the most effective method of isolating each polymorph was determined to be careful selection of solvent, concentration and crystallization vessel (Supporting Information 1.2). Isolation of each polymorph was determined via p-XRD and each system analyzed via UV-Vis spectroscopy, differential scanning calorimetry and low temperature p-XRD.

### ***Structural Motifs in Gm8m and Gm8p***

Despite the chemical diagram suggesting that both molecules will be planar, they adopt slightly different non-planar conformations in their polymorphs (Supporting Information Table 19). Even their *ab initio* optimized structures correspond to a non-planar molecule, which can be attributed to steric clashes between hydrogen atoms on C2 and the aromatic rings.

Gm8m – O crystallizes in the triclinic space group *P*-1. Through a double 1-3 ring stacking motif (**Figure 3a**), the 1-ring of each molecule forms close contacts with the 3-ring of another molecule, which have complementary electrostatic charges (**Figure 1**). These dimers are then packed together through 1-ring stacking and 3-ring stacking motifs to form 2D sheets, and subsequently the 3D crystal through cyclic CH $\cdots$ O=C and CH $\cdots$ NO<sub>2</sub> contacts (**Figure 3b**), and the cyclic CH $\cdots$ CH<sub>3</sub> and 1D-chain motifs. The molecular packing in Gm8m – O allows all molecules to be nearly coplanar, in contrast to Gm8m – Y and Gm8p polymorphs. The complete set of packing motifs for Gm8m – O is shown in Supporting Information Table 23.

Gm8m – Y crystallizes in the monoclinic space group *P*2<sub>1</sub>/*c*. Rather than the fully stacked dimer as that in Gm8m – O, there is only a half-stacking motif in Gm8m – Y (**Figure 3c**), with each molecule offset (~ 5 Å) by translation along the long axis of the other molecule, forming 1D stacks. These 1D stacks then pack through tilted motifs into zigzagging 2D

sheets, at an angle of  $64^\circ$  to each other, and eventually through cyclic  $\text{CH}\cdots\text{O}=\text{C}$  and  $\text{CH}\cdots\text{NO}_2$  contacts to the 3D crystal (**Figure 3d**). The complete packing motifs for  $\text{Gm8m} - \text{Y}$  are shown in Supporting Information Table 22. The only packing similarity between  $\text{Gm8m} - \text{Y}$  and  $\text{Gm8m} - \text{O}$  are the cyclic  $\text{CH}\cdots\text{O}=\text{C}$  and  $\text{CH}\cdots\text{NO}_2$  motifs (**Figure 3b and 3d**), so only 3 molecules out of a 15-molecule cluster can be overlaid ( $\text{RMSD}_3 = 0.441\text{\AA}$ ) using the structural similarity tool in Mercury.<sup>61</sup>

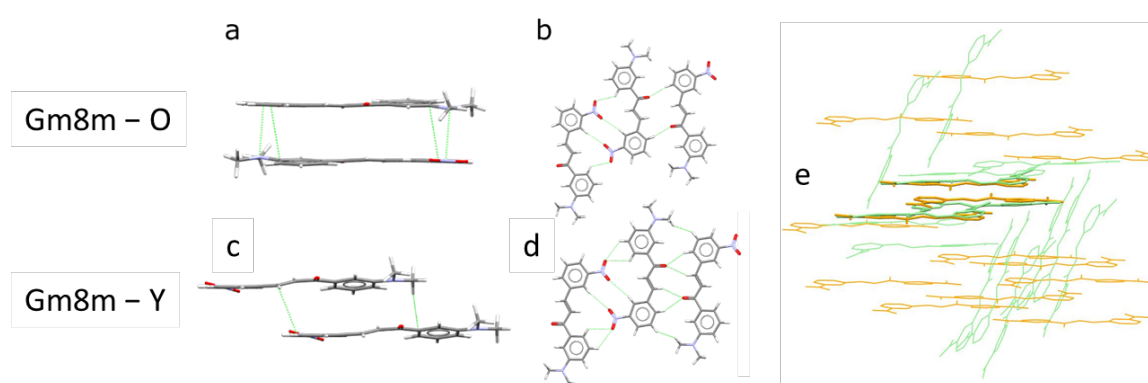


**Figure 3.** Packing motifs in  $\text{Gm8m} - \text{O}$  and  $\text{Gm8m} - \text{Y}$  (major component) with close contacts highlighted: a) the double 1-3 ring stacked dimer motif in  $\text{Gm8m} - \text{O}$ ; b) cyclic  $\text{CH}\cdots\text{O}=\text{C}$  and  $\text{CH}\cdots\text{NO}_2$  motifs in  $\text{Gm8m} - \text{O}$ ; c) half-stacking motif in  $\text{Gm8m} - \text{Y}$ ; d) cyclic  $\text{CH}\cdots\text{O}=\text{C}$  and  $\text{CH}\cdots\text{NO}_2$  motifs in  $\text{Gm8m} - \text{Y}$ ; e) 15-molecule overlay of  $\text{Gm8m} - \text{Y}$  (in green) and  $\text{Gm8m} - \text{O}$  (in orange), with the 3 overlaid molecules in thicker stick representation.

$\text{Gm8p} - \text{R}$  crystallizes in the monoclinic space group  $P2_1/n$ . The molecules pack into dimers with the double 1-3 ring-stacked motif (**Figure 4a**), but the “para” positions of the nitro groups means the dimer configuration is shifted along the short molecular axis relative to that in  $\text{Gm8m} - \text{O}$ . These dimers are linked via a cyclic  $\text{NO}_2\cdots\text{CH}_3$  motif to form 1D stacks (**Figure 4a and c**), which duplicate along the horizontal directions in **Figure 4e** into a

coplanar 2D sheet and then pack with adjacent sheets into a zigzagging 3D structure (**Figure 4e**). The zigzag appears along the short axis of the molecules, at an angle of  $83^\circ$ . The complete packing motifs for Gm8p – R are shown in Supporting Information Table 24.

Gm8p – B crystallizes in the monoclinic space group  $P2_1/c$ . The double 1-3 ring stacked dimer in Gm8p – R is again present in Gm8p – B (**Figure 4b**). However the continued packing in the direction of the 1D stack is mediated by a modified cyclic  $\text{NO}_2\dots\text{CH}_3$  motif, similar to that in Gm8p – R, but with larger ring overlaps between two adjacent dimers (**Figure 4d**). These 1D stacks form coplanar 2D sheets through translation along the long axis of the molecule, bringing the 1 and 3 rings of adjacent stacks side-by-side. Then 2D sheets interdigitate into the 3D structure with molecules in adjacent sheets lie in alternating molecular planes, at an angle of  $62^\circ$  (**Figure 4f**). The complete packing motifs for Gm8p – B are shown in Supporting Information Table 25. The packing of Gm8p – B and Gm8p – R can be seen as two alternative packings of the 1D stacks, which can either be translated along the short or the long axis of the molecules in the stacks (**Figure 4e and f**). The result is that between Gm8p – B and Gm8p – R, the only packing similarity is the 1D stack (**Figure 4e and f**), an overlay of 3 molecules out of a 15-molecule cluster.

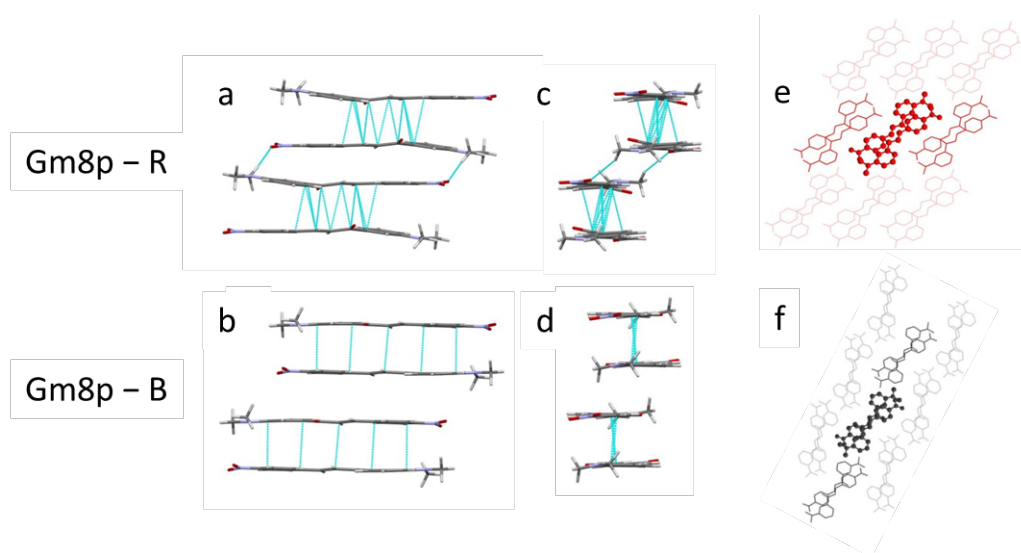


**Figure 4.** Packing motifs in Gm8p – R and Gm8p – B: a) the double 1-3 ring stacking motif in Gm8p – R and the cyclic NO<sub>2</sub>⋯CH<sub>3</sub> motif between two dimers; b) the double 1-3 ring stacking motif in Gm8p – B and the cyclic NO<sub>2</sub>⋯CH<sub>3</sub> motif between two dimers; c) side view of the cyclic NO<sub>2</sub>⋯CH<sub>3</sub> motif in Gm8p – R; d) side view of the modified cyclic NO<sub>2</sub>⋯CH<sub>3</sub> motif in Gm8p – B; e) packing of 1D stacks to coplanar 2D sheets and then to Gm8p – R; f) packing of 1D stacks to coplanar 2D sheets and then to Gm8p – B. Different shades indicate molecules in 2D sheets are not coplanar. The molecules in ball-and-stick representation are the three molecules that are in common in an overlay of Gm8p – R and Gm8p – B (RMSD<sub>3</sub> = 0.598 Å).

Among the four crystal structures, the double 1-3 ring stacking motif is only missing in the Gm8m – Y polymorph (**Figure 5**), whereas this is the most prominent  $\pi$ - $\pi$  stacking motif in each of the other structures.

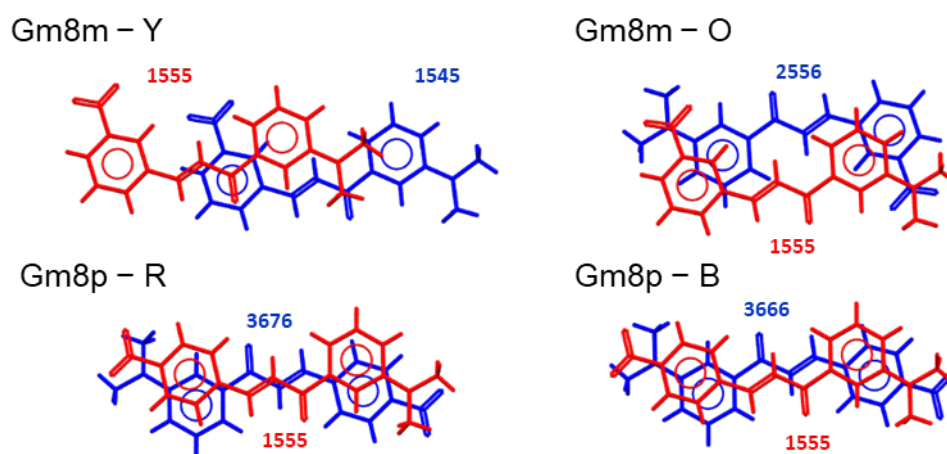


**Figure 5.** Stacking dimers for Gm8m and Gm8p polymorphs, showing the most prominent  $\pi$ - $\pi$  stacking motif in each structure. See Supporting Information 2.5.3.3 for the definition of ARU labels of the molecules.

## Thermal Analysis

To assess the thermodynamics of the four systems, differential scanning calorimetry measurements were carried out for each of the polymorphs of Gm8m and Gm8p (**Figure 6**, Supporting Information 1.7). Initially, thermographs were produced with ramp rates of  $5^{\circ}\text{C}\cdot\text{min}^{-1}$  and  $10^{\circ}\text{C}\cdot\text{min}^{-1}$ . In Gm8m – O an event involving an endotherm followed by an exotherm appears at  $93^{\circ}\text{C}$ , which precedes an endotherm at  $120^{\circ}\text{C}$ . As the thermogram of Gm8m – Y shows an endotherm at  $122^{\circ}\text{C}$ , it is likely that Gm8m – O transforms to Gm8m – Y on heating, and this endotherm is showing the melting of Gm8m – Y. Despite increasing the heating rate, the transformation at  $93^{\circ}\text{C}$  is sufficiently fast that it is impossible to determine whether this is a multi-stage transformation, or to measure the enthalpy of fusion of Gm8m – O. Therefore, we cannot deduce whether the two polymorphs are monotropically or enantiotropically related. Following the melt, Gm8m does not crystallize on cooling and instead forms an amorphous phase, as indicated by a glass transition at  $T_g = -3^{\circ}\text{C}$  (Supporting Information Figure 17).

In the thermogram of Gm8p – R, an endotherm appears at  $152^{\circ}\text{C}$  followed by a small exotherm with a further endotherm at  $167^{\circ}\text{C}$ . Gm8p – B shows only a single endothermic transition at  $167^{\circ}\text{C}$ . It is therefore likely that Gm8p – R is transforming to Gm8p – B, and the final endotherm in both cases is the melting of Gm8p – B. By assessing thermograms with higher ramp rates ( $20^{\circ}\text{C}\cdot\text{min}^{-1}$  –  $50^{\circ}\text{C}\cdot\text{min}^{-1}$ ), the melting of Gm8p – R with less contamination from recrystallization could be measured. The heat of fusion for Gm8p – R and Gm8p – B were measured at a ramp rate of  $50^{\circ}\text{C}\cdot\text{min}^{-1}$  to be  $93\text{ J}\cdot\text{g}^{-1}$  and  $116\text{ J}\cdot\text{g}^{-1}$  respectively, indicating from Burger's rules<sup>62</sup> that the system is monotropic, with Gm8p – B the more stable structure.

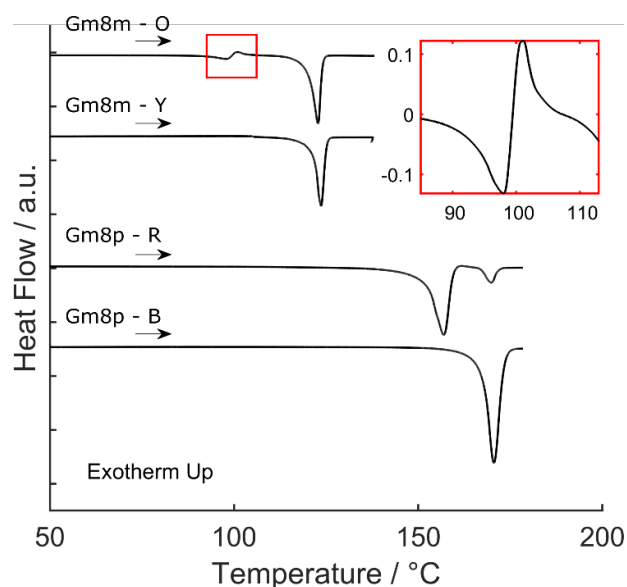


**Figure 6** Differential scanning calorimetry thermograms of Gm8m – O and Gm8m – Y (top) and Gm8p – R and Gm8p – B (Bottom). Inset shows an enlarged thermogram of the phase transition of Gm8m – O to Gm8m – Y, vertical axis units are  $\text{J}\cdot\text{g}^{-1}$ . The heating rate for Gm8m samples was  $5^\circ\text{C}\cdot\text{min}^{-1}$  and  $10^\circ\text{C}\cdot\text{min}^{-1}$  for Gm8p samples.

Periodic DFT-D calculations (Supporting Information 2.1-2.3) show that Gm8m – O is the most stable at low temperatures by only  $2\text{-}3\text{ kJ}\cdot\text{mol}^{-1}$ , but harmonic phonon calculations show that Gm8m – Y has a slightly higher entropy than Gm8m – O, so the relative free energy reduces with temperature. These calculations ignore the observed disorder and thermal expansion and the calculated differences are too small to determine whether the Gm8m polymorphs are monotropically or enantiotropically related. PBE-MBD\* predicts a large difference in the lattice energy between Gm8p – R and Gm8p – B, and all dispersion corrections have Gm8p – B being the more stable at low temperatures. Phonon calculations (Supporting Information Figure 29) show that the free energies would only become equal well above the melting point, correctly predicting the observed monotropic relationship.

Low temperature p-XRD data was collected to assess thermal behavior of all polymorphs down to 12 K, with changes in crystallographic cell parameters assessed by

refining the powder patterns with the solved crystal structures using Reitveld refinement (Supporting Information 1.5). Gm8m – Y, Gm8m – O and Gm8p – R showed no indication of polymorphic change between 300 K and 12 K, apart from continuous thermal contraction and expansion of the cell axes across the whole temperature range. In contrast, during the cooling and heating of Gm8p – B a rapid change in the diffraction peak positions was seen around 110-170 K, over a temperature range too small to represent thermal lattice contraction. This suggests a transition between a low temperature (LT) and a high temperature (HT) form of Gm8p – B (Supporting Information 1.5 and Supporting Information Figure 9), which will be referred to as Gm8p – B<sub>HT</sub>. To assess the differences in Gm8p – B crystal structures, before and after the p-XRD changes, sc-XRD was taken of the Gm8p – B polymorph at 100 K (Gm8p – B) and 240 K (Gm8p – B<sub>HT</sub>, Supporting Information Table 15), which show that the change in structure is subtle, with an RMSD<sub>20</sub> = 0.533 Å (Supporting Information Figure 8). Generated powder patterns from these structures matched well with the powder data taken above and below the transition. Ab-initio optimization of Gm8p – B<sub>HT</sub> resulted in the same lattice energy minimum as the low temperature form, indicating the HT form of Gm8p – B is thermally stabilized.

## **CRYSTALLOCHROMY OF Gm8m & Gm8p**

### ***UV-Vis Analysis***

The UV-Vis absorption of Gm8m and Gm8p polymorphs in the solid-state is analyzed via diffuse reflectance with the application of the Kubelka-Munk transformation.<sup>63</sup> **Figure 7** shows a comparison of the absorption of the powdered samples, which show a clear change in the onset of absorption and a variable broadening of the high wavelength peak between the polymorphs. The absorption onset extracted using the Kubelka-Munk transformation varies from 2.45 eV to 2.11 eV between Gm8m – Y and Gm8p – B, as expected from the color of

the crystals (Supporting Information 1.8.2). The solutions are pale yellow for Gm8m and a darker yellow/orange for Gm8p, with only small changes in UV-Vis wavelengths in different solvents varying in polarity (ethyl acetate, toluene, ethanol and chloroform, Supporting Information 1.8 and Figure 20). It was also observed that Gm8m – Y crystals are fluorescent upon UV illumination (Supporting Information 1.9).

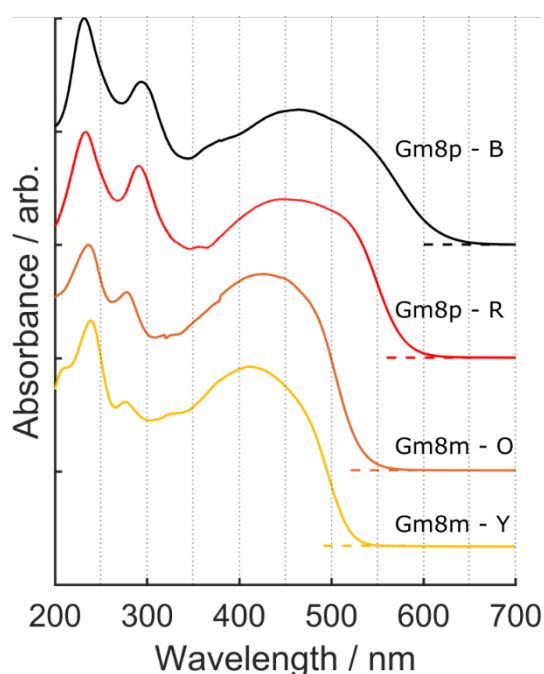


**Figure 7.** The UV-Vis absorption of powders of Gm8m and Gm8p polymorphs observed via the Kubelka-Munk transformation of measured diffuse reflectance. The baselines are offset for clarity.

### *Cluster TD-DFT Calculations*

To account for the differences in color between the polymorphs of Gm8m and Gm8p (**Figure 2** and **Figure 7**), we performed TD-DFT ( $\omega$ B97x) calculations of the absorption spectra of isolated molecules, dimers, stacks and small clusters cut from the four crystal structures.

The variations in conformation between the molecules in the different polymorphs make very little difference to the delocalized orbitals (Supporting Information 2.5.2), and the TD-

DFT calculated UV-Vis spectra of the monomers in the Gm8m and Gm8p polymorphs only red-shift slightly compared to the isolated molecules and to a similar extent (**Figure 8**), (Supporting Information Figure 31). The HOMO-1 – LUMO transition is much stronger than the HOMO-LUMO transition and varies more between Gm8m and Gm8p as it has more density on the NO<sub>2</sub> groups (Supporting Information Table 21) and so conformational changes cannot account for the color difference between the pairs of polymorphs. However, there are considerable red-shifts of the spectrum when the chalcone molecules form a double 1-3 ring dimer motif (**Figure 8** and Supporting Information 2.5.3), existing in Gm8m – O, Gm8p – B and Gm8p – R (**Figure 5**), but not in Gm8m – Y. In contrast, the only  $\pi$ -stacking motif in Gm8m – Y (**Figure 3c**), was found to blue-shift the absorption. Further investigations of larger stacks of the most red-shifting motifs in the polymorphs, and 15-molecule clusters (**Figure 8**) show that both Gm8m – O and Gm8p – B benefit from a cumulative effect in which the red-shifts were enhanced by the stacking of the most red-shifting dimer motif, while in Gm8p – R this cumulative effect does not exist. Thus, the significant difference in color for the pair of polymorphs of Gm8m arises from the double 1-3 ring stacking motif in the orange polymorph, further enhanced by a cumulative effect. In the pair of Gm8p polymorphs, the color difference is largely the result of the absence of the cumulative effect in Gm8p – R.

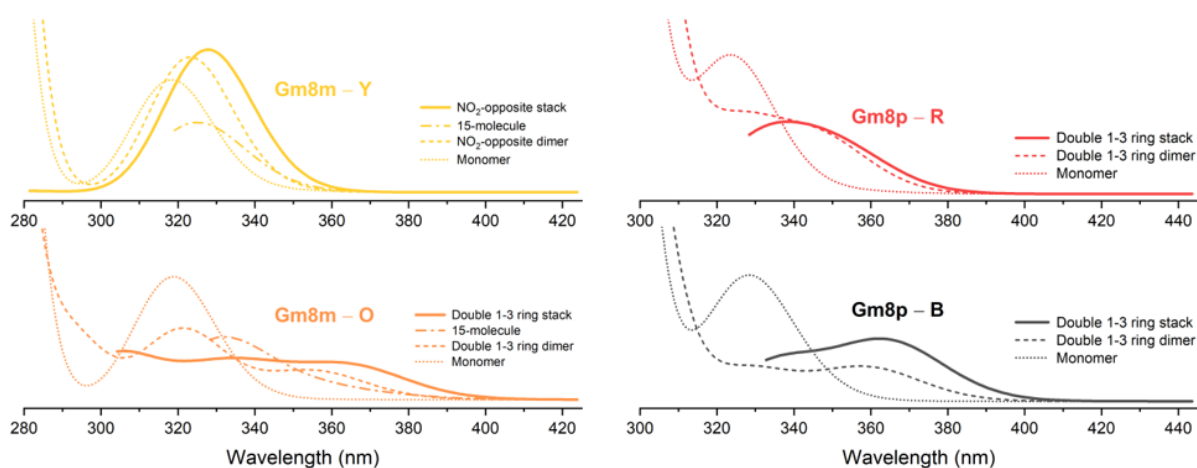


**Figure 8.** The calculated UV-Vis spectra of Gm8m and Gm8p polymorphs showing the effects of molecular conformation (dotted lines), dimerization (dash lines), 15-molecular clusters (Gm8m only, dash-dotted lines) and stacks of strongest red-shifting dimer motifs (solid lines). See Supporting Information 2.5 for details of TD-DFT calculations.

## DISCUSSION

We have found and structurally characterized two polymorphs of two isomers of dimethylamino-nitro chalcone. The *meta*-nitro isomer crystallizes as an orange (Gm8m – O) or yellow polymorph (Gm8m – Y), and sometimes a concomitant mixture, depending on solvent and the container used for the ambient crystallization (Supporting Information 1.2). Gm8m – Y shows significant dynamic disorder in the position of the NO<sub>2</sub> group, increasing at higher temperatures. The *para*-nitro isomer predominantly crystallized in the red polymorph (Gm8p – R), with either a needle, plate or block morphology, but a black polymorph (Gm8p – B) has been obtained from acetone and toluene, sometimes concomitantly. Low temperature p-XRD highlighted a rapid change in the p-XRD pattern of Gm8p – B around 110 K, but as the high and low temperature structures are very similar (Supporting Information Table 15), corresponding to the same lattice energy minimum, it is debatable whether this should be classified as a polymorph.<sup>64</sup> Further study could determine

whether the discontinuity in lattice parameters (Supporting Information Figure 9) correlates with a change in the dynamical motion of the molecules. A third sample of Gm8p has been observed (Supporting Information 1.2 and Table 3), which is orange in color, but only samples of low crystallinity have been obtained, with 3D electron diffraction (ED)<sup>60</sup> allowing an estimate of two different sets of cell parameters (Supporting Information 1.6). The combination of p-XRD and electron diffraction with a limited crystal structure prediction study<sup>65, 66</sup> (Supporting Information 1.6), suggests that the orange sample contains crystals that are based on a stacking motif similar to that seen in Gm8p – B. **Figure 9** summarizes the solid form landscape established so far. The color of the crystals considerably aids the detection of polymorphism, but the extent of screening for polymorphs performed is only a start on what would be involved in an industrial polymorph screen.<sup>67-69</sup> However, these new systems already show the experimental challenges of characterizing these polymorphic systems.

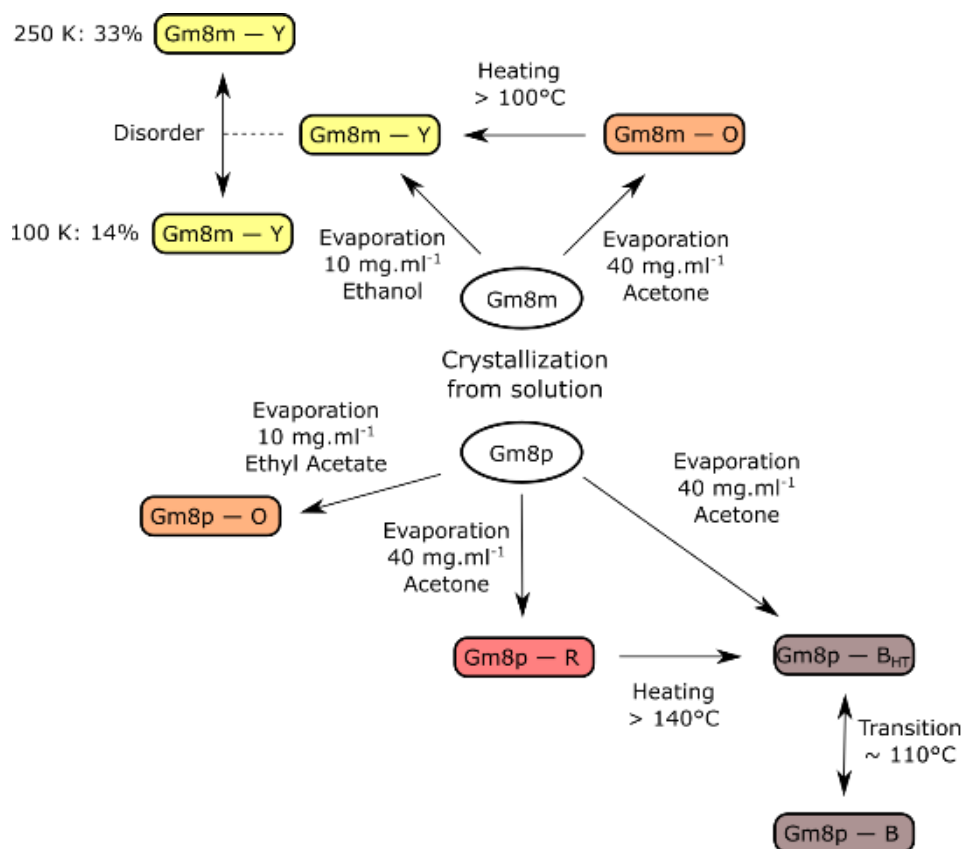


**Figure 9** Experimental solid form landscape of Gm8m and Gm8p, summarizing the forms discovered by solvent screen and interconversion revealed through DSC and low temperature p-XRD.

Phase pure crystallization of these molecules is difficult as the crystal form produced from evaporative growth is highly sensitive to changes in solvent, concentration and crystallization vessel (Supporting Information 1.2). Concomitant crystallization is often observed, and even solvent evaporative crystallization has not always equilibrated to a phase pure sample. This suggests that both pairs of polymorphs are close in thermodynamic stability around ambient, and kinetic factors are important in determining which polymorph is seen.

Experiments show a monotropic relationship between Gm8p - B and Gm8p - R with Gm8p - B being the more stable, but there is a change to a lower energy form below 110K that is so subtle that it cannot be modelled by lattice energy minimization. The

thermodynamic relationship between Gm8m – Y and Gm8m – O cannot be determined by our DSC measurements, and further experiments utilizing concurrent synchrotron p-XRD-DSC<sup>70</sup> are needed to determine the mechanism of the transformation. There is clearly a barrier to this solid-state transformation. Computationally, the standard periodic DFT-D calculations with the usual PBE functional confirm that Gm8m – O and Gm8p – B are the more stable forms at low temperature, though this result may be affected by the delocalization error in the PBE functional.<sup>43</sup> Calculations of the harmonic phonon spectra of the polymorphs show that the free energy differences reduce with increasing temperature. However Gm8m – Y shows considerable anisotropy in the thermal expansion (Supporting Information Table 14) and so it is likely that the differences in thermal expansion of the polymorphs will affect the calculations of the relative stability.<sup>71</sup> The temperature dependent disorder in Gm8m – Y (Supporting Information 1.4) will also stabilize it, and is not included in current computational models.

The observation of different morphologies of Gm8p – R in different solvents (Supporting Information 1.2) emphasize the role of variable growth kinetics in the crystallization of Gm8p, and show that improvements on the simple predictions of morphology based on interplanar spacings<sup>72</sup> (Supporting Information Figures 58 and 59) would need to include the solvent.<sup>73,74</sup>

A kinetic barrier for solid-state transformation between the polymorphs arises from the substantial differences in their crystal packing, which is suggested by the differences in color that reflect the different close contact dimers (Supporting Information 2.5.3). We have been able to account for the color differences in terms of the contributions of different dimers and then larger stacks of molecules within the crystal, with almost all the nearest neighbor molecules within the crystals producing some change to the solid-state spectrum (Supporting Information 2.5.3.4). Furthermore, the calculated spectra can shift significantly when certain

dimer interactions are extended into larger stacks (Supporting Information 2.5.4). The color differences are not caused by these structures being conformational polymorphs, though this would also generally be associated with a kinetic barrier to a solid-state transformation.<sup>75</sup> These polymorphs show the challenges in predicting the optical properties of organic crystals. We were not able to afford the TD-DFT calculations of a cluster containing all the contact dimer interactions for Gm8p – B, and it was challenging to do those on the 15 molecule clusters for Gm8m polymorphs (Supporting Information 2.5.4.3). Hence, converging cluster and stack calculations is not a practical strategy for quantitative prediction of the UV-Vis spectra of large flexible organic crystals. This will require the use of periodic TD-DFT calculations with an adequate functional, such as  $\omega$ B97x, which is, as far as we are aware, not yet implemented in any code.

The reported properties of these sets of polymorphs highlight the challenges in predicting all the properties of pharmaceutical polymorphs from the crystal structure, and hence in computationally quantifying the inter-relationship between structure, properties, processing and performance of a pharmaceutical product.<sup>76</sup>

## CONCLUSION

The *meta*- and *para*-nitro isomers of dimethylamino-nitro chalcone (Gm8m and Gm8p) exhibit crystallochromy and the corresponding crystal structures have been determined, along with their corresponding UV-Vis spectra. The limited polymorph solvent crystallization screen shows a complex dependence of the polymorph and morphology on the solvent and crystallization vessel, with both systems being capable of showing concomitant crystallization. The polymorphic phase transitions are kinetically hindered, making it difficult to establish the thermodynamic relationship between Gm8m – O and Gm8m – Y experimentally. There is evidence of a third polymorph of Gm8p, which has been partially

structurally characterized using the complimentary techniques of 3D electron diffraction and crystal structure prediction.

We have shown that the trends in the colors of the crystals can be explained by TD-DFT calculations on dimers, stacks and clusters, but that the complex balance of these contributions means that quantitative predictions of the absorption spectra of pharmaceutical crystals are not possible with currently available computational chemistry methods. Concomitant polymorphism and solid-state transitions have been observed in both Gm8m and Gm8p, underlining the importance of the interplay between kinetics and thermodynamics in polymorphic systems. Thus, this is a valuable model polymorphic system for investigation of the relationship between crystal structures and their physical properties, thermodynamic and kinetic stability, particularly because of the ease of polymorph identification provided by the conveniently distinguishable colors.

## **ASSOCIATED CONTENT**

### **Supporting Information**

**Experimental (section 1):** synthesis (1.1), solvent screen (1.2), crystallographic tables (1.3), disorder in Gm8m – Y (1.4), low temperature p-XRD (1.5), characterization of the orange form of Gm8p (1.6), thermal analysis (1.7), UV-Vis spectroscopy (1.8), Fluorescence spectroscopy (1.9).

**Computational (section 2):** periodic DFT-D structural optimization (2.1), periodic DFT-D relative energies using various dispersion corrections (2.2), phonon dispersion and free energy calculations (2.3), example of electronic optical gap (Gm8m – Y) by periodic PBE calculations (2.4), dimer and cluster color calculations (2.5), calculation of diamagnetic susceptibility tensors (2.6).

### **Accession Codes**

CCDC 1983901-1983910 contains the supplementary crystallographic data for this paper. These data can be obtained free of charge from The Cambridge Crystallographic Data Centre via [www.ccdc.cam.ac.uk/structures](http://www.ccdc.cam.ac.uk/structures).

### **AUTHOR INFORMATION**

Corresponding Author

Simon R. Hall, School of Chemistry, University of Bristol, BS8 1TS.

simon.hall@bristol.ac.uk

### **Author Contributions**

The manuscript was written through contributions of all authors. All authors have given approval to the final version of the manuscript.

### **Funding Sources**

MagnaPharm is a collaborative research project funded by the European Union's Horizon 2020 Research and Innovation programme under grant agreement number 736899. This work used the ARCHER UK National Supercomputing Service (<http://www.archer.ac.uk>) via our membership of the UK's HEC Materials Chemistry Consortium, which is funded by EPSRC (EP/L000202, EP/R029431). MAZ acknowledges EPSRC (EP/N004884/1) for funding. CLH acknowledges EPSRC (EP/L015544/1) for funding.

### **ACKNOWLEDGMENT**

The authors would like to thank Dr Asma Buanz (UCL) for assistance and helpful discussions regarding the interpretation of the thermal analysis data; Dr. Liam Willbraham (UCL) for a script to produce the UV-Vis spectrum from Gaussian output; Mr Benjamin Cole (UCL) for preliminary work on the color calculations; Dr Louise S. Price (UCL) for the crystal structure

prediction calculations and discussions. The chalcones were synthesized in Gonzaga by Dr G. D'Ambruoso, J. Drexelius, S. Econonmu, K. Gallo, R. Getnet, J. Hazen, C. Hicks, Dr J. Krause, Dr M. Matsumoto, S. Paeth, and M. Shea.

## ABBREVIATIONS

**Gm8m**: meta nitro isomer of (E)-3'-dimethylamino-nitrochalcone

**Gm8p**: para nitro isomer of (E)-3'-dimethylamino-nitrochalcone

## REFERENCES

1. Hilfiker, R., *Polymorphism in the Pharmaceutical Industry*. Wiley-VCH: Weinheim, 2006.
2. Bernstein, J., *Polymorphism in Molecular Crystals*. Clarendon Press: Oxford, 2002.
3. Nyman, J.; Yu, L.; Reutzel-Edens, S. M., Accuracy and reproducibility in crystal structure prediction: the curious case of ROY. *CrystEngComm* **2019**, *21*, 2080-2088.
4. Gushurst, K.; Nyman, J.; Boerrigter, S., The PO13 crystal structure of ROY. *CrystEngComm* **2019**, *21*, 1363-1368.
5. Tan, M.; Shtukenberg, A.; Zhu, S.; Xu, W.; Dooryhee, E.; Nichols, S.; Ward, M.; Kahr, B.; Zhu, Q., ROY revisited, again: the eighth solved structure. *Faraday Discuss.* **2018**, *211*, 477-491.
6. Yu, L., Polymorphism in Molecular Solids: An Extraordinary System of Red, Orange, and Yellow Crystals. *Acc. Chem. Res.* **2010**, *43*, 1257-1266.
7. Zhuang, C. L.; Zhang, W.; Sheng, C. Q.; Zhang, W. N.; Xing, C. G.; Miao, Z. Y., Chalcone: A Privileged Structure in Medicinal Chemistry. *Chem. Rev.* **2017**, *117*, 7762-7810.
8. Aoki, N.; Muko, M.; Ohta, E.; Ohta, S., C-geranylated chalcones from the stems of *Angelica keiskei* with superoxide-scavenging activity. *J. Nat. Prod.* **2008**, *71*, 1308-1310.
9. Nowakowska, Z., A review of anti-infective and anti-inflammatory chalcones. *Eur. J. Med. Chem.* **2007**, *42*, 125-137.
10. Nielsen, S. F.; Boesen, T.; Larsen, M.; Schonning, K.; Kromann, H., Antibacterial chalcones-bioisosteric replacement of the 4'-hydroxy group. *Bioorg. & Med. Chem.* **2004**, *12*, 3047-3054.
11. Shigeru, M.; Makoto, M.; Hironaka, A.; Susumu, O., Inhibition of gastric H<sup>+</sup>,K<sup>+</sup>-ATPase by the anti-ulcer agent, sofalcone. *Biochem. Pharmacol.* **1991**, *42*, 1447-1451.
12. Szliszka, E.; Czuba, P. Z.; Mazur, B.; Sedek, L.; Paradysz, A.; Krol, W., Chalcones Enhance TRAIL-Induced Apoptosis in Prostate Cancer Cells. *Int. J. of Mol. Sci.* **2010**, *11*, 1-13.
13. Ducki, S., Antimitotic Chalcones and Related Compounds as Inhibitors of Tubulin Assembly. *Anti-Cancer Agents Med. Chem.* **2009**, *9*, 336-347.
14. Liang, C.; Peng, S.; Li, J.; Lu, J.; Guan, D.; Jiang, F.; Lu, C.; Li, F.; He, X.; Zhu, H.; Au, D. W. T.; Yang, D.; Zhang, B.-T.; Lu, A.; Zhang, G., Inhibition of osteoblastic Smurf1 promotes bone formation in mouse models of distinctive age-related osteoporosis. *Nat. Commun.* **2018**, *9*, 3428.

15. Mahapatra, D. K.; Asati, V.; Bharti, S. K., Chalcones and their therapeutic targets for the management of diabetes: Structural and pharmacological perspectives. *Eur. J. of Med. Chem.* **2015**, *92*, 839-865.
16. Iwamura, C.; Shinoda, K.; Yoshimura, M.; Watanabe, Y.; Obata, A.; Nakayama, T., Naringenin Chalcone Suppresses Allergic Asthma by Inhibiting the Type-2 Function of CD4 T Cells. *Allergol. Int.* **2010**, *59*, 67-73.
17. Vanangamudi, G.; Subramanian, M.; Thirunarayanan, G., Synthesis, spectral linearity, antimicrobial, antioxidant and insect antifeedant activities of some 2,5-dimethyl-3-thienyl chalcones. *Arabian J. of Chem.* **2017**, *10*, S1254-S1266.
18. Wan, Z. H.; Hu, D. Y.; Li, P.; Xie, D. D.; Gan, X. H., Synthesis, Antiviral Bioactivity of Novel 4-Thioquinazoline Derivatives Containing Chalcone Moiety. *Molecules* **2015**, *20*, 11861-11874.
19. Batovska, D. I.; Todorova, I., Trends in Utilization of the Pharmacological Potential of Chalcones. *Curr. Clin. Pharmacol.* **2010**, *5*, 1-29.
20. Sahu, N. K.; Balbhadra, S. S.; Choudhary, J.; Kohli, D. V., Exploring Pharmacological Significance of Chalcone Scaffold: A Review. *Cur. Med. Chem.* **2012**, *19*, 209-225.
21. Sharifzadeh, S.; Darancet, P.; Kronik, L.; Neaton, J., Low-Energy Charge-Transfer Excitons in Organic Solids from First-Principles: The Case of Pentacene. *J. of Phys. Chem. Lett.* **2013**, *4*, 2197-2201.
22. Sharifzadeh, S.; Biller, A.; Kronik, L.; Neaton, J., Quasiparticle and optical spectroscopy of the organic semiconductors pentacene and PTCDA from first principles. *Phys. Rev. B* **2012**, *85*, 125307.
23. Li, J.; D'Avino, G.; Duchemin, I.; Beljonne, D.; Blase, X., Combining the Many-Body GW Formalism with Classical Polarizable Models: Insights on the Electronic Structure of Molecular Solids. *J. of Phys. Chem. Lett.* **2016**, *7*, 2814-2820.
24. Rao, A.; Wilson, M.; Albert-Seifried, S.; Di Pietro, R.; Friend, R., Photophysics of pentacene thin films: The role of exciton fission and heating effects. *Phys. Rev. B* **2011**, *84*, 195411.
25. Klebe, G.; Graser, F.; Hadicke, E.; Berndt, J., Crystallochromy as a solid state effect - Correlation of molecular conformation, crystal packing and color in perylene-3,4,9,10-bis(dicarboximide) pigments. *Acta Crystallogr., Sect. B: Struct. Sci.* **1989**, *45*, 69-77.
26. Kazmaier, P. M.; Hoffmann, R., A Theoretical Study of Crystallochromy - Quantum Interference Effects in the Spectra of Perylene Pigments. *J. Am. Chem. Soc.* **1994**, *116*, 9684-9691.
27. Nogueira, B. A.; Castiglioni, C.; Fausto, R., Color polymorphism in organic crystals. *Commun. Chem.* **2020**, *3*, 34-34.
28. Stephenson, G. A.; Borchardt, T. B.; Byrn, S. R.; Bowyer, J.; Bunnell, C. A.; Snorek, S. V.; Yu, L., Conformational and Color Polymorphism of 5-Methyl-2-[(2-Nitrophenyl)Amino]-3-Thiophenecarbonitrile. *J. Pharm. Sci.* **1995**, *84*, 1385-1386.
29. Fletton, R. A.; Lancaster, R. W.; Harris, R. K.; Kenwright, A. M.; Packer, K. J.; Waters, D. N.; Yeadon, A., A comparative spectroscopic investigation of 2 polymorphs of 4'-methyl-2'-nitroacetanilide using solid-state infrared and high resolution solid-state nuclear-magnetic-resonance spectroscopy. *J. of the Chem. Soc., Perkin Trans. 2* **1986**, 1705-1709.
30. Li, H.; Stowell, J. G.; Borchardt, T. B.; Byrn, S. R., Synthesis, Conformational Polymorphism, and Construction of a G-T Diagram of 2-[(2-Nitrophenyl)amino]-3-thiophenecarbonitrile. *Cryst. Growth Des.* **2006**, *6*, 2469-2474.
31. Harty, E. L.; Ha, A. R.; Warren, M. R.; Thompson, A. L.; Allan, D. R.; Goodwin, A. L.; Funnell, N. P., Reversible piezochromism in a molecular wine-rack. *Chem. Commun.* **2015**, *51*, 10608-10611.

32. Braun, D. E.; Gelbrich, T.; Jetty, R. K. R.; Kahlenberg, V.; Price, S. L.; Griesser, U. J., Colored polymorphs: Thermochemical and structural features of N-picryl-p-toluidine polymorphs and solvates. *Cryst. Growth Des.* **2008**, *8*, 1977-1989.
33. Sangtani, E.; Sahu, S. K.; Thorat, S. H.; Gawade, R. L.; Jha, K. K.; Munshi, P.; Gonnade, R. G., Furosemide Cocrystals with Pyridines: An Interesting Case of Color Cocrystal Polymorphism. *Cryst. Growth Des.* **2015**, *15*, 5858-5872.
34. Sangtani, E.; Mandal, S. K.; Sreelakshmi, A. S.; Munshi, P.; Gonnade, R. G., Salts and Cocrystals of Furosemide with Pyridines: Differences in  $\pi$ -Stacking and Color Polymorphism. *Cryst. Growth Des.* **2017**, *17*, 3071-3087.
35. Bruker, A. X. S. I. *SAINT+*, 6.45; Madison, Wisconsin, USA, 2003.
36. Sheldrick, G. M. *SADABS Bruker AXS area detector scaling and absorption correction*, Bruker Analytical X-ray Instruments Inc., Madison, Wisconsin, USA, University of Gottingen: Gottingen, Germany, 2001.
37. Dolomanov, O. V.; Bourhis, L. J.; Gildea, R. J.; Howard, J. A. K.; Puschmann, H., OLEX2: a complete structure solution, refinement and analysis program. *J. Appl. Crystallogr.* **2009**, *42*, 339-341.
38. Palatinus, L.; Chapuis, G., SUPERFLIP - a computer program for the solution of crystal structures by charge flipping in arbitrary dimensions. *J. of Appl. Crystallogr.* **2007**, *40*, 786-790.
39. Palatinus, L.; Prathapa, S.; van Smaalen, S., EDMA: a computer program for topological analysis of discrete electron densities. *J. of Appl. Crystallogr.* **2012**, *45*, 575-580.
40. Sheldrick, G. M., A short history of SHELX. *Acta Crystallogr., Sect. A: Found. Crystallogr.* **2008**, *64*, 112-122.
41. Macrae, C. F.; Edgington, P. R.; McCabe, P.; Pidcock, E.; Shields, G. P.; Taylor, R.; Towler, M.; van de Streek, J., Mercury: visualization and analysis of crystal structures. *J. of Appl. Crystallogr.* **2006**, *39*, 453-457.
42. Hoja, J.; Ko, H.-Y.; Neumann, M. A.; Car, R.; DiStasio, R. A.; Tkatchenko, A., Reliable and practical computational description of molecular crystal polymorphs. *Sci. Adv.* **2019**, *5*, eaau-3338.
43. LeBlanc, L.; Dale, S.; Taylor, C.; Becke, A.; Day, G.; Johnson, E., Pervasive Delocalisation Error Causes Spurious Proton Transfer in Organic Acid-Base Co-Crystals. *Angew. Chem., Int. Ed.* **2018**, *57*, 14906-14910.
44. Mortazavi, M.; Hoja, J.; Aerts, L.; Quere, L.; van de Streek, J.; Neumann, M. A.; Tkatchenko, A., Computational polymorph screening reveals late-appearing and poorly-soluble form of rotigotine. *Commun. Chem.* **2019**, *2*, 70.
45. Clark, S. J.; Segall, M. D.; Pickard, C. J.; Hasnip, P. J.; Probert, M. J.; Refson, K.; Payne, M. C., First principles methods using CASTEP. *Z. Kristallogr. Cryst. Mater.* **2005**, *220*, 567-570.
46. Perdew, J. P.; Ruzsinszky, A.; Tao, J. M.; Staroverov, V. N.; Scuseria, G. E.; Csonka, G. I., Prescription for the design and selection of density functional approximations: More constraint satisfaction with fewer fits. *J. of Chem. Phys.* **2005**, *123*, 062201.
47. Tkatchenko, A.; Scheffler, M., Accurate Molecular Van Der Waals Interactions from Ground-State Electron Density and Free-Atom Reference Data. *Phys. Rev. Lett.* **2009**, *102*, 073005.
48. Tkatchenko, A.; DiStasio, R. A. J.; Car, R.; Scheffler, M., Accurate and efficient method for many-body van der Waals interactions. *Phys. Rev. Lett.* **2012**, *108*, 236402.
49. Grimme, S., Semiempirical GGA-type density functional constructed with a long-range dispersion correction. *J. Comput. Chem.* **2006**, *27*, 1787-1799.

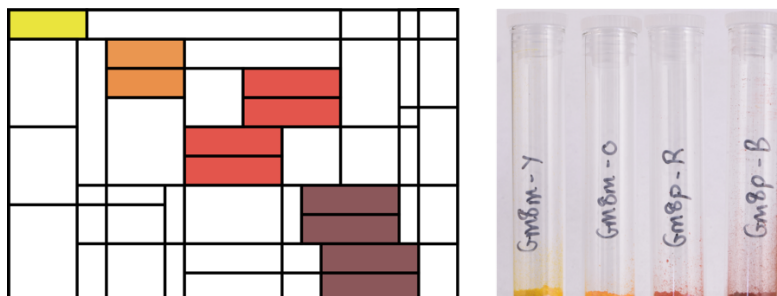
50. Grimme, S.; Antony, J.; Ehrlich, S.; Krieg, H., A consistent and accurate ab initio parametrization of density functional dispersion correction (DFT-D) for the 94 elements H-Pu. *J. Chem. Phys.* **2010**, *132*, 154104.
51. Guo, R.; Uddin, M. N.; Price, L. S.; Price, S. L., Calculation of Diamagnetic Susceptibility Tensors of Organic Crystals: From Coronene to Pharmaceutical Polymorphs. *J. Phys. Chem. A* **2020**, *124*, 1409-1420.
52. Perdew, J. P., Density functional theory and the band gap problem. *Int. J. Quantum Chem.* **1985**, *28*, 497-523.
53. Frisch, M. J.; Trucks, G. W.; Schlegel, H. B.; Scuseria, G. E.; Robb, M. A.; Cheeseman, J. R.; Scalmani, G.; Barone, V.; Mennucci, B.; Petersson, G. A.; Nakatsuji, H.; Caricato, M.; Li, X.; Hratchian, H. P.; Izmaylov, A. F.; Bloino, J.; Zheng, G.; Sonnenberg, J. L.; Hada, M.; Ehara, M.; Toyota, K.; Fukuda, R.; Hasegawa, J.; Ishida, M.; Nakajima, T.; Honda, Y.; Kitao, O.; Nakai, H.; Vreven, T.; Montgomery, J. A., Jr; Peralta, J. E.; Ogliaro, F.; Bearpark, M.; Heyd, J. J.; Brothers, E.; Kudin, K. N.; Staroverov, V. N.; Kobayashi, R.; Normand, J.; Raghavachari, K.; Rendell, A.; Burant, J. C.; Iyengar, S. S.; Tomasi, J.; Cossi, M.; Rega, N.; Millam, J. M.; Klene, M.; Knox, J. E.; Cross, J. B.; Bakken, V.; Adamo, C.; Jaramillo, J.; Gomperts, R.; Stratmann, R. E.; Yazyev, O.; Austin, A. J.; Cammi, R.; Pomelli, C.; Ochterski, J. W.; Martin, R. L.; Morokuma, K.; Zakrzewski, V. G.; Voth, G. A.; Salvador, P.; Dannenberg, J. J.; Dapprich, S.; Daniels, A. D.; Farkas, Ö.; Foresman, J. B.; Ortiz, J. V.; Cioslowski, J.; Fox, D. J. *Gaussian 09, Revision D.01*, 2009.
54. Furche, F.; Ahlrichs, R.; Hattig, C.; Klopper, W.; Sierka, M.; Weigend, F., Turbomole. *Wiley Interdiscip. Rev.: Comput. Mol. Sci.* **2014**, *4*, 91-100.
55. Chai, J.; Head-Gordon, M., Systematic optimization of long-range corrected hybrid density functionals. *J. Chem. Phys.* **2008**, *128*, 084106.
56. Hehre, W. J.; Ditchfie, R.; Pople, J. A., Self-Consistent Molecular-Orbital Methods .12. Further Extensions of Gaussian-Type Basis Sets for Use in Molecular-Orbital Studies of Organic-Molecules. *J. Chem. Phys.* **1972**, *56*, 2257-2261.
57. Jacquemin, D.; Moore, B.; Planchat, A.; Adamo, C.; Autschbach, J., Performance of an Optimally Tuned Range-Separated Hybrid Functional for 0–0 Electronic Excitation Energies. *J. Chem. Theory Comput.* **2014**, *10*, 1677-1685.
58. Peach, M. J. G.; Benfield, P.; Helgaker, T.; Tozer, D. J., Excitation energies in density functional theory: An evaluation and a diagnostic test. *J. Chem. Phys.* **2008**, *128*, 44118-44118.
59. Dennington, R.; Keith, T.; Millam, J. *GaussView*, *5*; 2009.
60. Gemmi, M.; Mugnaioli, E.; Gorelik, T. E.; Kolb, U.; Palatinus, L.; Boullay, P.; Hovmöller, S.; Abrahams, J. P., 3D Electron Diffraction: The Nanocrystallography Revolution. *ACS Cent. Sci.* **2019**, *5*, 1315-1329.
61. Macrae, C. F.; Bruno, I. J.; Chisholm, J. A.; Edgington, P. R.; McCabe, P.; Pidcock, E.; Rodriguez-Monge, L.; Taylor, R.; van de Streek, J.; Wood, P. A., Mercury CSD 2.0 - new features for the visualization and investigation of crystal structures. *J. Appl. Crystallogr.* **2008**, *41*, 466-470.
62. Burger, A.; Ramberger, R., Polymorphism of Pharmaceuticals and Other Molecular-Crystals .1. Theory of Thermodynamic Rules. *Mikrochim. Acta* **1979**, *2*, 259-271.
63. Kubelka, P.; Munk; F.Z., Ein Beitrag zur Optik der Farbanstriche. *Z. Tech. Phys.* **1931**, *12*, 593-601.
64. Gavezzotti, A., A solid-state chemist's view of the crystal polymorphism of organic compounds. *J. Pharm. Sci.* **2007**, *96*, 2232-2241.
65. Price, S. L., Predicting crystal structures of organic compounds. *Chem. Soc. Rev.* **2014**, *43*, 2098-2111.

66. Pantelides, C. C.; Adjiman, C. S.; Kazantsev, A. V., General Computational Algorithms for Ab Initio Crystal Structure Prediction for Organic Molecules. *Top. Curr. Chem.* **2014**, *345*, 25-58.
67. Bhardwaj, R. M.; McMahon, J. A.; Nyman, J.; Price, L. S.; Konar, S.; Oswald, I. D. H.; Pulham, C. R.; Price, S. L.; Reutzel-Edens, S. M., A Prolific Solvate Former, Galunisertib, under the Pressure of Crystal Structure Prediction, Produces Ten Diverse Polymorphs. *J. Am. Chem. Soc.* **2019**, *141*, 13887-13897.
68. Lee, A. Y.; Erdemir, D.; Myerson, A. S., Crystal Polymorphism in Chemical Process Development. *Annu. Rev. of Chem. and Biomol. Eng., Vol 2* **2011**, *2*, 259-280.
69. Newman, A., Specialized Solid Form Screening Techniques. *Org. Process Res. Dev.* **2013**, *17*, 457-471.
70. Clout, A.; Buanz, A. B. M.; Prior, T. J.; Reinhard, C.; Wu, Y.; O'Hare, D.; Williams, G. R.; Gaisford, S., Simultaneous Differential Scanning Calorimetry-Synchrotron X-ray Powder Diffraction: A Powerful Technique for Physical Form Characterization in Pharmaceutical Materials. *Anal. Chem.* **2016**, *88*, 10111-10117.
71. Brandenburg, J. G.; Potticary, J.; Sparkes, H. A.; Price, S. L.; Hall, S. R., Thermal Expansion of Carbamazepine: Systematic Crystallographic Measurements Challenge Quantum Chemical Calculations. *J. Phys. Chem. Lett.* **2017**, *8*, 4319-4324.
72. Donnay, J. D. H.; Harker, D., A new law of crystal morphology extending the Law of Bravais. *Am. Mineral.* **1937**, *22*, 446-467.
73. Sun, Y. Y.; Tilbury, C. J.; Reutzel-Edens, S. M.; Bhardwaj, R. M.; Li, J. J.; Doherty, M. F., Modeling Olanzapine Solution Growth Morphologies. *Cryst. Growth Des.* **2018**, *18*, 905-911.
74. Tilbury, C.; Joswiak, M.; Peters, B.; Doherty, M., Modeling Step Velocities and Edge Surface Structures during Growth of Non-Centrosymmetric Crystals. *Cryst. Growth Des.* **2017**, *17*, 2066-2080.
75. Srirambhatla, V. K.; Guo, R.; Dawson, D. M.; Price, S. L.; Florence, A. J., Reversible, Two-Step Single-Crystal to Single-Crystal Phase Transitions between Desloratadine Forms I, II, and III. *Cryst. Growth Des.* **2020**, *20*, 1800-1810.
76. Sun, C. C., Material Science Tetrahedron-A Useful Tool for Pharmaceutical Research and Development. *J. Pharm. Sci.* **2009**, *98*, 1671-1687.

For Table of Contents Use Only.

### Color Differences Highlight Concomitant Polymorphism of Chalcones

Charlie L. Hall<sup>1</sup>, Rui Guo<sup>2</sup>, Jason Potticary<sup>1</sup>, Matthew E. Cremeens<sup>3</sup>, Stephen D. Warren<sup>3</sup>, Iryna Andrusenko<sup>4</sup>, Mauro Gemmi<sup>4</sup>, Martijn A. Zwijnenburg<sup>2</sup>, Hazel A. Sparkes<sup>1</sup>, Natalie E. Pridmore<sup>1</sup>, Sarah L. Price<sup>2</sup>, Simon R. Hall<sup>1\*</sup>



The *meta*- and *para*- nitro isomers of (*E*)-3'-dimethylamino-nitrochalcone are shown to exhibit concomitant color polymorphism, with crystals varying in colour across the optical spectrum. To assess the effect of molecular configuration and crystal packing on the colors of crystals, time dependent DFT calculations were carried out on a variety of small clusters cut from the crystal structures of the four polymorphs.